CHIN. PHYS. LETT. Vol. 33, No. 8 (2016) 087303

Energy Levels of Coupled Plasmonic Cavities *

Chuan-Pu Liu(刘传普)[1], Xin-Li Zhu(朱新利)[1], Jia-Sen Zhang(张家森)[1,2**], Jun Xu(徐军)[1], Yamin Leprince-Wang(王亚敏)[3], Da-Peng Yu(俞大鹏)[1,2**]

[1]*State Key Laboratory for Mesoscopic Physics, Department of Physics, Peking University, Beijing 100871*
[2]*Collaborative Innovation Center of Quantum Matter, Beijing 100871*
[3]*Université Paris-Est, Laboratoire ESYCOM, UPEM, Marne-la-Vallée 77454, France*

(Received 6 June 2016)

We demonstrate the hybridization of the plasmonic modes in directly coupled whispering gallery cavities fabricated on silver films and present the mode patterns and energy levels using cathodoluminescence spectroscopy. Although the energy of the most antisymmetrically coupled modes is higher than that of the corresponding symmetrically coupled ones, the contrary cases happen for small quantum number modes. We attribute the phenomenon to the different surface plasmon polariton paths between the symmetrically and antisymmetrically coupled modes. These results provide an understanding of the resonant properties in coupled plasmonic cavities, which have potential applications in nanophotonic devices.

PACS: 73.20.Mf, 42.79.−e, 42.82.−m, 42.82.Gw DOI: 10.1088/0256-307X/33/8/087303

Surface plasmon polaritons (SPPs) are an electromagnetic surface wave coupled to free electron plasma in metals.[1] Advancements that design and manipulate the geometry of metallic structures enable us to control SPP properties and to tailor them for many applications, such as solar cells, SERS, high resolution microscopy, and drug designs.[2−5] As a fundamental building block of future nanophotonic devices and integrated optical circuits, plasmonic cavities, which offer the ability to confine an optical field in a small volume below the wavelength of light using metallic nanostructures, attract more attention. Hofmann *et al.*[6] imaged plasmonic modes of annular nanoresonators by spectrally resolved cathodoluminescence (CL). Controlled squeezing of visible light into nanometer-sized optical cavities has been realized via a metal–insulator–metal (MIM) structure and an ultrasmall mode volume is achieved.[7,8] Hao *et al.*[9] observed the effects of symmetry breaking in a metallic nanostructure consisting of a disk inside a ring, resulting in a tunable fano resonance. Vesseur *et al.*[10−12] investigated the plasmonic whispering gallery cavities based on a circular groove in a Au surface and showed that it can be used as versatile antennas to control spontaneous emission. Our group[13−16] came up with a template stripping method to produce an ultrasmooth surface and systematically studied different kinds of plasmonic modes in open cavities. Plasmonic cavities showed wide applications in spontaneous emission enhancement,[17−20] SERS,[21,22] solar cells,[23] and other fields.[24−31] However, there are no detailed works on how plasmonic cavities interact with each other, and the resonant properties of coupled plasmonic cavities remain unknown. Meanwhile, plasmon hybridization[32] between various coupled metallic nanostructures, such as nanoshells,[33] nanoparticle dimers,[34−36] and oligomers,[37−41] has been studied extensively. In these structures, the energy of the antisymmetrically coupled mode is usually higher than that of the corresponding symmetrically coupled mode.

In this Letter, we systematically investigate the resonant wavelength and plasmonic modes of coupled whispering gallery cavities (CWGCs) using spatially resolved CL. The in-phase and anti-phase hybridizations of the plasmonic modes of two single whispering gallery cavities (SWGCs) result in symmetrically and antisymmetrically coupled modes, respectively. The energy of the antisymmetrically coupled modes is still not higher than that of the symmetrically coupled ones. According to the resonant conditions in whispering gallery (WG) cavities, a model is proposed to explain the evolution of the plasmon energy levels in the CWGCs. These results provide an understanding of hybridization of plasmonic modes in coupled cavities, and show a method to control the resonant properties.

A poly (methyl methacrylate) (PMMA) film with thickness of 500 nm on a silicon substrate was exposed and developed into the desired nanostructures by electron beam lithography (EBL). A silver layer, which was larger than the thickness of the PMMA, was then deposited on the patterns via magnetron sputtering deposition. After that, the metal film was glued to another silicon wafer with an epoxy resin adhesive. Due to the weak adhesion between the metal and the PMMA, the silver layer can be easily stripped off from the PMMA surface. After removing the residual PMMA in acetone, the resulting metal layer completely inherited the smoothness and the morphology of the PMMA patterns.

A scanning electron microscope (SEM) equipped with a lithography attachment (Raith Elphy Plus) was used to perform EBL. The nanostructures on the sil-

*Supported by the National Basic Research Program of China under Grant No 2013CB932602, and the National Natural Science Foundation of China under Grant Nos 11574011, 61377050 and 11234001.
**Corresponding author. Email: yudp@pku.edu.cn; jszhang@pku.edu.cn
© 2016 Chinese Physical Society and IOP Publishing Ltd

ver film were characterized by an SEM (FEI company, DB235 and Quanta 200F).

By combining an SEM (FEI Quanta 200F) and a CL (Gatan Mono CL 3+) detection system, we carried out spatially and spectrally resolved CL measurements of the plasmonic modes of the cavities. SPPs were excited on the undersurface of the cavities by using a 30 KeV electron beam of the SEM. The scattering light was collected by a parabolic mirror above a sample holder and led to a spectrometer. In the experiment, the acquisition time of all the CL spectra was 16 s.

A commercial finite-difference time-domain (FDTD) solver (Lumerical FDTD solution 8.6) with a mesh of 2 nm and simulation boundaries of perfectly matched layers were used to obtain the simulations. A Drude model was locally fitted to the experimentally obtained optical constants of Ag.[42] A waveguide mode of the SPPs was launched in the cavities directly.

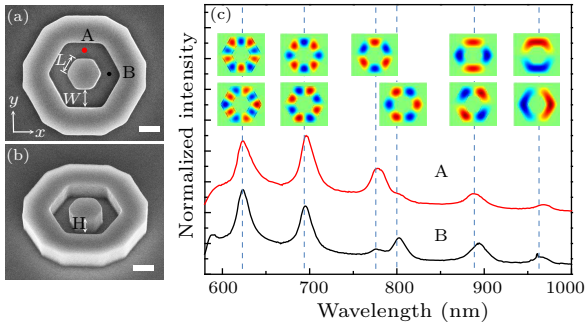

Fig. 1. (a) Top-view and (b) 45-degree-tilted SEM images of a single plasmonic whispering gallery cavity with L = 450 nm, W =430 nm, and H =500 nm. Scale bars are 500 nm. (c) CL spectra when the electron beam is launched at A and B points in (a). The insets are the corresponding calculated mode patterns.

To couple metallic cavities effectively, we consider regular hexagon plasmonic WG cavities with rectangular metallic grooves. The cavities were fabricated on a silver film by using the template stripping method we previously developed.[14] First, SWGCs are studied, and Figs. 1(a) and 1(b) show the top-view and 45-degree-tilted SEM images of a typical SWGC. The silver groove with a width W of 430 nm acts as a plasmonic waveguide, and the side length L of the pillar at the center of the cavity is 450 nm. The height H of the pillar and the wall is 500 nm. The fabrication method produces an ultra-smooth metal surface, a precipitous top-to-bottom profile, and an ideal geometry, which are of importance in investigating the SPP behavior in cavities.

In the experiment, SPPs were launched by using the electron beam of a CL spectroscopy, which served as a plasmonic point source. The scattering light from the cavity was collected and its spectrum was measured. The spectra when the electron beam was impinged vertically at two points A and B in Fig. 1(a) are shown in Fig. 1(c) in the wavelength range of 600–1000 nm. There are four common resonant wavelengths at 968 nm, 890 nm, 696 nm and 624 nm between the two spectra. They have different resonant peaks around 800 nm, which are located at 778 nm and 802 nm.

Due to the fact that the mode patterns of the SWGNs cannot be obtained from the CL, we calculated the resonant mode patterns of the out-of-plane electric field component of the SPPs on the undersurface of the cavity with the same geometry as the experiment using the FDTD method. The simulated plasmonic mode patterns were plotted as insets in Fig. 1(c), in which the blue dashed lines indicate the corresponding resonant peaks. The mode patterns in the upper row have even parity with respect to the y-axis, while the mode patterns in the lower row have odd parity. Here integer m denotes the azimuthal symmetry number relative to the rotational axis perpendicular to the cavity surface. Thus the modes of the upper and lower rows from right to left are $m^{\rm e} = 1$, 2, 3, 4 and 5, and $m^{\rm o} = 1$, 2, 3, 4 and 5 modes, respectively, where the superscripts indicate the parity corresponding to 'even' and 'odd'. Although the experimental resonant wavelengths have slight deviation, the even and odd parity modes with the same symmetry number are degenerate pairs except the $m^{\rm e} = 3^{\rm e}$ and $m^{\rm o} = 3^{\rm o}$ modes, which are a non-degenerate pair. Following the nomenclature in Refs. [43], the modes $m^{\rm e} = 1$, 2, 4 and 5, and $m^{\rm o} = 1$, 2, 4 and 5 are a-type modes with two symmetry lines while the modes $m^{\rm e} = 3$ and $m^{\rm o} = 3$ are b-type modes with six symmetry lines. It has been demonstrated that the a-type modes always appear in degenerate pairs and the b-type modes do not form degenerate pairs.[43,44]

For the plasmonic modes in the hexagonal WG cavities, we can decompose the vector of the SPPs into two orthogonal components, $\boldsymbol{k}_1$ and $\boldsymbol{k}_2$, which are perpendicular and parallel to the edge of the cavity and correspond to the standing wave mode and traveling wave mode, respectively. Ignoring the penetration of the SPPs into the silver wall, the resonance conditions are given by $k_1 W = 2\pi n$ and $k_2 C_{\rm eff} = 2\pi p$, where n and p are quantum numbers, and $C_{\rm eff}$ is the effective path of the SPPs in the cavity. The vector number of the SPPs $k_{\rm SPP} = \sqrt{k_1^2 + k_2^2}$. Here we only consider the fundamental standing wave modes, i.e., $n = 1$. Therefore, $\lambda_{\rm SPP}$ is given by

$$\lambda_{\rm SPP} = \frac{2C_{\rm eff}W}{\sqrt{C_{\rm eff}^2 + 4p^2W^2}}. \quad (1)$$

To study the hybridization of plasmonic WG cavities, we fabricated coupled cavities with two identical WG cavities sharing one side of a groove, and Figs. 2(a) and 2(b) show their top-view and 45-degree-tilted SEM images, respectively. The width of the groove is 430 nm, as well as the separation between the two pillars. The side length and the height of the pillars are 450 nm and 500 nm, respectively. The height of the silver wall is also 500 nm. We launched SPPs at three points A, B, and C in Fig. 2(a) according to the symmetry of the coupled cavities and the CL spectra are shown in Fig. 2(c). Line B has more peaks than the other two.

When a mode pattern has a zero intensity at the incident point of the electron beam, it cannot be launched. As a result, the modes in line A are symmetric with respect to the y-axis, and line C cannot include antisymmetric modes with respect to the x-axis. Line C is slightly red shifted due to the sample distorting under the electron beam's impact during the spectra acquisition.

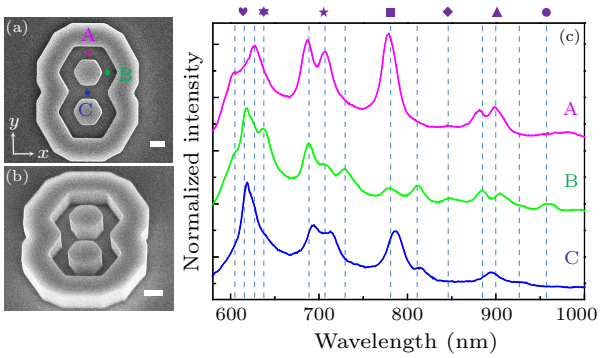

Fig. 2. (a) Top-view and (b) 45-degree-tilted SEM images of the coupled plasmonic WG cavities. The cavity height is 500 nm. Scale bars are 500 nm. (c) CL spectra when the electron beam is launched at A, B, and C points in (a).

To determine the patterns of the resonant modes of the coupled cavities, we measured the CL spectra when the incident position of the electron beam was located along the middle line of the groove of the hexagon, including the common side of the two WG cavities. Along each side, 10 spectra were obtained, which were used to compose the patterns of the resonant modes. According to the symmetry of the coupled cavities, four line-scan spectra were enough to characterize all the eleven side grooves of the cavity. For each mode the intensities of the spectra were normalized by setting the smallest value as 0 and the largest value as 1. After interpolating 10 points into 100 for each side to smooth the intensities of each mode, we used the normalized CL spectra to compose the mode patterns. Figure 3 shows the mode patterns corresponding to the resonant peaks in Fig. 2(c) in the wavelength range of 600–1000 nm. The modes can be seen as the hybridization results of the modes of two SWGNs due to two kinds of coupling: in-phase and anti-phase couplings, resulting in the symmetric (bonding) and antisymmetric (antibonding) modes, respectively. We used + to symbolize in-phase coupling and − anti-phase coupling. Thus the two modes of Figs. 3(d) and 3(c) are called $(2^{e}+2^{e})$ and $(2^{e}-2^{e})$, which have symmetric and antisymmetric distributions of the amplitudes of the electric field with respect to the x-axis, respectively. The bonding state $(2^{e}+2^{e})$ has a maximum intensity at the center of the shared groove due to the constructive interference. On the contrary, the intensity of the antibonding state at the same point is always zero. There are 8 symmetric modes in Fig. 3, including Figs. 3(b), 3(d), 3(f), 3(g), 3(i), 3(j), 3(l) and 3(m). Other patterns belong to the antisymmetric modes.

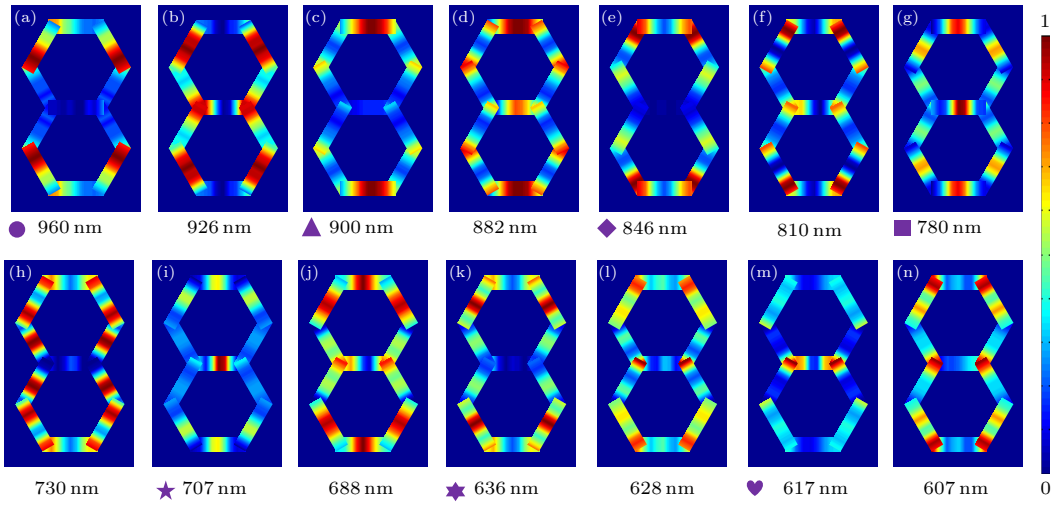

Fig. 3. (a)–(n) Mode patterns of the coupled plasmonic WG cavities obtained from the CL spectra. The intensities are normalized.

To assign the resonant patterns in Fig. 3 clearly, we calculated the mode patterns of a CWGC with the same geometry in the experiment using the FDTD method and the results are shown in Fig. 4. The modes in Figs. 4(a)–4(p) are assigned to the modes $(1^{o}-1^{o})$, $(2^{o}+2^{o})$, $(2^{e}-2^{e})$, $(2^{e}+2^{e})$, $(2^{o}-2^{o})$, $(3^{o}+3^{o})$, $(3^{e}+3^{e})$, $(3^{e}-3^{e})$, $(3^{o}-3^{o})$, $(4^{e}+4^{e})$, $(4^{o}+4^{o})$, $(4^{e}-4^{e})$ $(4^{o}-4^{o})$, $(5^{e}+5^{e})$, $(5^{o}+5^{o})$ and $(5^{e}-5^{e})$, respectively. The resonant wavelengths of the symmetrically and antisymmetrically hybridized pair are different except for the modes $(3^{e}+3^{e})$ (Fig. 4(g)) and $(3^{e}-3^{e})$ (Fig. 4(h)), which have the same resonant wavelength.

Compared with the numerical mode patterns, we can assign the experimental ones. Figures 3(a)–3(n) clearly match Figs. 4(a)–4(p), respectively. The experiment cannot give the respective mode patterns of the degenerate modes. Thus we mixed the simulated patterns of the modes $(3^{e}+3^{e})$ and $(3^{e}-3^{e})$ and show it in Fig. 4(q), which is in accordance with Fig. 3(g). An-

other difference between the experimental results and the simulation is the patterns of the modes $(4^{e}-4^{e})$ and $(4^{o}+4^{o})$. In the experiment, their resonant wavelengths cannot be distinguished and only a mixed mode pattern was obtained (Fig. 3(j)). We mixed the mode patterns of the modes $(4^{e}-4^{e})$ (Fig. 4(l)) and $(4^{o}+4^{o})$ (Fig. 4(k)) into one mode pattern and show it in Fig. 4(r), which corresponds to Fig. 3(j).

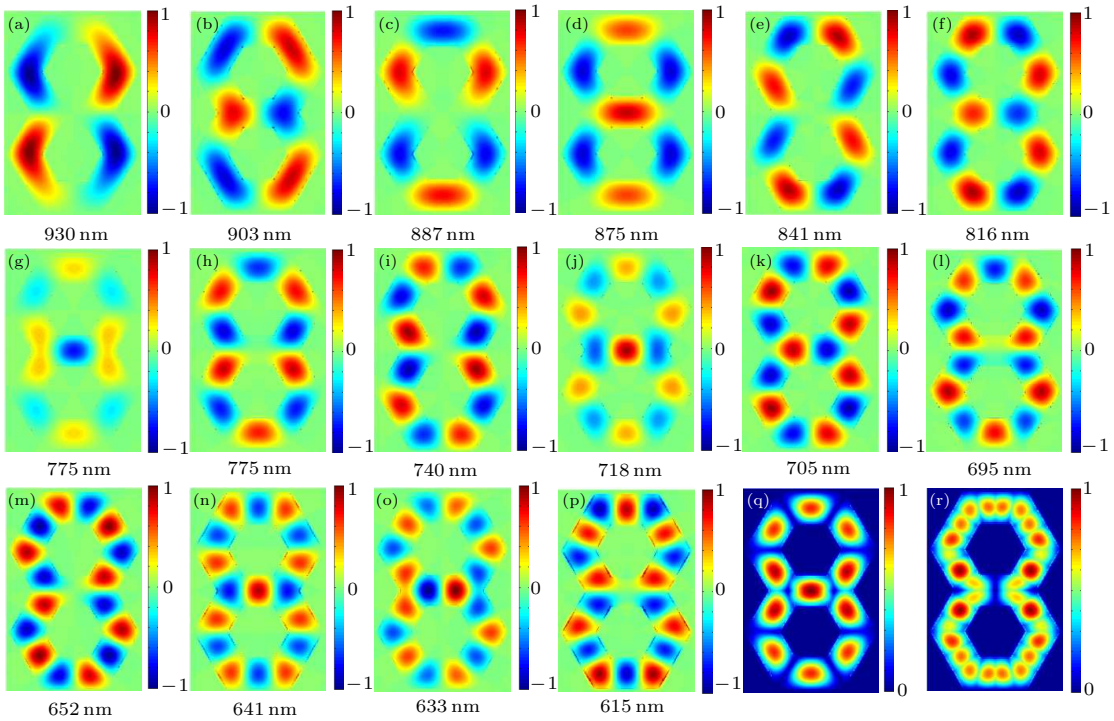

Fig. 4. (a)–(p) Simulated mode patterns of the coupled plasmonic WG cavities. (q) Mixed pattern of (g) and (h). (r) Mixed pattern of (k) and (l). Here (g) and (h) are of the same wavelength but different symmetries in the y direction.

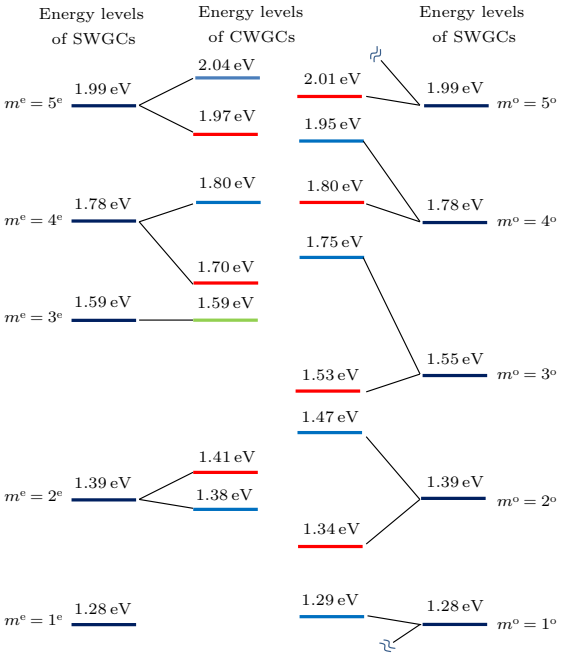

Fig. 5. Experimental energy levels of the single plasmonic cavity and the coupled cavities. The numbers above the levels denote the resonant energy. The blue lines indicate the antisymmetrically coupled modes and the red ones the symmetrically coupled modes. The green line at 1.59 eV represents the degenerated $(3^{e}\pm 3^{e})$ modes.

An SWGC, of which mode patterns are very similar to the delocalized π orbitals of the six lowest energy states of the benzene molecule C_6H_6,[45] can be considered as an artificial plasmonic atom. Thus the CWGCs are artificial plasmonic diatomic molecules. In real molecules, the energy level of the antibonding state is always higher than the bonding state. The principle is not applied for the plasmonic molecules. The experimental energy levels of the plasmonic atom and molecule are shown in Fig. 5. The blue levels indicate antisymmetrically coupled modes, and the red ones are symmetrically coupled modes. The plasmon energies of the modes $(3^{e}+3^{e})$ and $(3^{e}-3^{e})$ degenerate at 1.59 eV, labeled by the green line of the molecular energy level, which is equal to energy of the mode 3^{e} of the SWGN. The energy of the antibonding mode $(2^{e}-2^{e})$ is less than bonding mode $(2^{e}+2^{e})$. Such a case also happens for the coupling of $m^{e}=1^{e}$ mode according to the simulation results. For the hybridization of other modes in Fig. 5, the energy of the antisymmetrically coupled modes is higher than that of the corresponding symmetrically coupled modes.

We approximated the effective path of SPPs as the perimeter of the middle line of the groove. The in-phase and anti-phase couplings have 8- and 0-shaped paths, respectively. Therefore C_{eff} is given by

$$C_{\text{eff}} \approx \begin{cases} 6L+2\sqrt{3}W, & \text{SWGCs}, \\ 12L+4\sqrt{3}W, & \text{inphase coupling}, \\ 10L+\frac{10\sqrt{3}}{3}W, & \text{antiphase coupling}. \end{cases} \quad (2)$$

The quantum number p is given by

$$p = \begin{cases} m, & \text{SWGCs}, \\ 2m, & \text{inphase coupling of even modes}, \\ 2m-1, & \text{antiphase couling of even modes}, \\ 2m, & \text{coupling of odd modes}. \end{cases} \tag{3}$$

Using Eq. (1) we can obtain that the modes $(3^{\rm e}+3^{\rm e})$ and $(3^{\rm e}-3^{\rm e})$ have the same $\lambda_{\rm SPP}$, resulting in degenerate states, and $\lambda_{\rm SPP}$ of the antisymmetrically coupled states of $m^{\rm e}=1^{\rm e}$ and $2^{\rm e}$ are larger than that of the corresponding symmetrically coupled states. Equation (1) can also explain the other results in Fig. 5. These characteristics of the coupled cavities originate from the different SPP paths between the symmetric and antisymmetric couplings and give a new way to control the resonant wavelength of coupled cavities.

In conclusion, we have demonstrated the resonant properties of the directly coupled plasmonic regular hexagon cavities. The hybridization of the two single cavity modes results in symmetrically and antisymmetrically coupled modes, of which the resonant energy depends on their quantum number and propagating path. Unlike the hybridizations in other systems, e.g., in real molecules, the energy of antisymmetrically coupled modes (antibonding states) with a small quantum number can be smaller than that of the corresponding symmetrically coupled modes (bonding states). Considering the different SPP paths between the symmetrically and antisymmetrically coupled modes, a model was used to explain the energy level of the coupled cavities. These results provide an understanding of the resonant properties of directly coupled plasmonic cavities, and show a method to tailor the resonance in plasmonic cavities.

References

[1] Raether H 1988 *Surface Plasmons on Smooth and Rough Surfaces and on Gratings* (Berlin: Springer-Verlag) p 4
[2] Maier S A 2007 *Plasmonics: Fundamentals and Applications* (Berlin: Springer-Verlag)
[3] Schuller J A, Barnard E S, Cai W et al 2010 *Nat. Mater.* **9** 193
[4] Linic S, Christopher P and Ingram D B 2011 *Nat. Mater.* **10** 911
[5] Berini P and De Leon I 2011 *Nat. Photon.* **6** 16
[6] Hofmann C E, Vesseur E J R, Sweatlock L A et al 2007 *Nano Lett.* **7** 3612
[7] Miyazaki H T and Kurokawa Y 2006 *Phys. Rev. Lett.* **96** 097401
[8] Kuttge M, Garciía de Abajo F J and Polman A 2010 *Nano Lett.* **10** 1537
[9] Hao F, Sonnefraud Y, Dorpe P V et al 2008 *Nano Lett.* **8** 3983
[10] Kuttge M, Vesseur E and Polman A 2009 *Appl. Phys. Lett.* **94** 183104
[11] Vesseur E J R and Polman A 2011 *Nano Lett.* **11** 5524
[12] Vesseur E J R and Polman A 2011 *Appl. Phys. Lett.* **99** 231112
[13] Zhu X L, Ma Y, Zhang J S et al 2010 *Phys. Rev. Lett.* **105** 127402
[14] Zhu X, Zhang Y, Zhang J et al 2010 *Adv. Mater.* **22** 4345
[15] Zhu X, Zhang J, Xu J et al 2011 *Nano Lett.* **11** 1117
[16] Zhu X L, Zhang J S, Xu J et al 2011 *ACS Nano* **5** 6546
[17] Russell K J, Liu T L, Cui S et al 2012 *Nat. Photon.* **6** 459
[18] Elvira D, Braive R, Beaudoin G et al 2013 *Appl. Phys. Lett.* **103** 061113
[19] Choy J T, Bulu I, Hausmann B J M et al 2013 *Appl. Phys. Lett.* **103** 161101
[20] Jiang J J, Xie Y B, Liu Z Y et al 2014 *Opt. Lett.* **39** 2378
[21] Heeg S, Oikonomou A, Fernandez-Garcia R et al 2014 *Nano Lett.* **14** 1762
[22] Im H, Bantz K C, Lee S H et al 2013 *Adv. Mater.* **25** 2678
[23] Chou S Y and Ding W 2013 *Opt. Express* **21** A60
[24] Raza S, Stenger N, Pors A et al 2014 *Nat. Commun.* **5** 4125
[25] Busson M P and Bidault S 2014 *Nano Lett.* **14** 284
[26] Dyer G C, Aizin G R, Preu S et al 2012 *Phys. Rev. Lett.* **109** 126803
[27] Chanda D, Shigeta K, Truong T et al 2011 *Nat. Commun.* **2** 479
[28] Kwon S H, Kang J H, Seassal C et al 2010 *Nano Lett.* **10** 3679
[29] Ameling R and Giessen H 2010 *Nano Lett.* **10** 4394
[30] Seo M K, Kwon S H, Ee H S et al 2009 *Nano Lett.* **9** 4078
[31] Weeber J C, Bouhelier A, Colas des F G et al 2007 *Nano Lett.* **7** 1352
[32] Prodan E, Radloff C, Halas N et al 2003 *Science* **302** 419
[33] Lassiter J B, Aizpurua J, Hernandez L I et al 2008 *Nano Lett.* **8** 1212
[34] Nordlander P, Oubre C, Prodan E et al 2004 *Nano Lett.* **4** 899
[35] Romero I, Aizpurua J, Bryant G W et al 2006 *Opt. Express* **14** 9988
[36] Brown L V, Sobhani H, Lassiter J B et al 2010 *ACS Nano* **4** 819
[37] Mirin N A, Bao K and Nordlander P 2009 *J. Phys. Chem. A* **113** 4028
[38] Liu N, Mukherjee S, Bao K et al 2012 *Nano Lett.* **12** 364
[39] Lassiter J B, Sobhani H, Knight M W et al 2012 *Nano Lett.* **12** 1058
[40] Luk'yanchuk B, Zheludev N I, Maier S A et al 2010 *Nat. Mater.* **9** 707
[41] Frimmer M, Coenen T and Koenderink A F 2012 *Phys. Rev. Lett.* **108** 077404
[42] Palik E D 1985 *Handbook of Optical Constants of Solids* (Orlando: Academic Press)
[43] Nobis T and Grundmann M 2005 *Phys. Rev.* A **72** 063806
[44] Wiersig J 2003 *Phys. Rev.* A **67** 023807
[45] Christoffersen R E 1971 *J. Am. Chem. Soc.* **93** 4104